Femto-molar detection of cancer marker-protein based on immuno-nanoplasmonics at single-nanoparticle scale

2016 Nanotechnology 27 185103

(http://iopscience.iop.org/0957-4484/27/18/185103)

IOP Publishing Nanotechnology
Nanotechnology 27 (2016) 185103 (7pp) doi:10.1088/0957-4484/27/18/185103

Femto-molar detection of cancer marker-protein based on immuno-nanoplasmonics at single-nanoparticle scale

Yoochan Hong[1], Eugene Lee[1,2], Minhee Ku[1,3], Jin-Suck Suh[1,4], Dae Sung Yoon[5] and Jaemoon Yang[1,4]

[1] Department of Radiology, College of Medicine, Yonsei University, Seoul 03722, Korea
[2] Nanomedical National Core Research Center, Yonsei University, Seoul 03722, Korea
[3] Brain Korea 21 PLUS Project for Medical Science, Yonsei University, Seoul 03722, Korea
[4] YUHS-KRIBB Medical Convergence Research Center, Yonsei University, Seoul 03722, Korea
[5] School of Biomedical Engineering, Korea University, Seoul 02841, Korea

E-mail: 177hum@yuhs.ac

Received 18 November 2015, revised 22 February 2016
Accepted for publication 4 March 2016
Published 24 March 2016

Abstract

We describe an *in vitro* biomarker sensor based on immuno-silver nanomarbles (iSNMs) and the nanoscattering spectrum imaging analysis system using localized surface plasmon resonance (LSPR). In particular, highly monodisperse SNMs with large figures of merit are prepared, and the sensing substrates are also fabricated using the nanoparticle adsorption method. The high sensitivity of the LSPR sensor based on an SNM is confirmed using various solvents that have different refractive indexes. For the sensitive and specific detection of epithelial cell adhesion molecules (EpCAMs) expressed on cancer cells, the surface of the SNM is conjugated with an anti-EpCAM aptamer, and molecular sensing for the EpCAM expression level is carried out using whole cell lysates from various cancer cell lines. Collectively, we have developed a biomarker-detectable LSPR sensor based on iSNMs, which allows for the sensitive and effective detection of EpCAMs at both the single-cell and femto-molar level.

S Online supplementary data available from stacks.iop.org/NANO/27/185103/mmedia

Keywords: localized surface plasmon resonance, silver nanomarble, aptamer, cancer, single nanoparticle spectroscopy

(Some figures may appear in colour only in the online journal)

1. Introduction

In recent years, biomarkers have gained immense scientific clinical value as well as interest in the practice of medicine, and also emerged as potentially important diagnostic tools for cancer and other diseases [1]. Because disease or cancer heterogeneity might be inherent in biomarkers and evaluation processes, it is important that their identification and quantification should proceed in various systematic ways [2–6]. Among the diverse methods, localized surface plasmon resonance (LSPR)-based optical nanobiosensors are considered one of the most powerful tools in the fields of biosensors and biotechnology [7–13]. LSPR possesses the specific characteristics of metallic or metalized nanostructured materials, such as noble metal nanoparticles, which can be excited by irradiation with incident photons and is resonant with the collective oscillations of conduction electrons at a specific wavelength [14–17]. To fabricate a well-behaved nanobiosensor based on LSPR for sensitive biomarker detection, the following conditions must be present. First of all, it is essential that the nanoparticles should be able to generate LSPR, and also have a large-value figure of merit (FOM). Moreover, it should be possible to make a substrate that is composed of nanoparticles easily, and the nanoparticles should be able to capture the target markers sensitively and specifically. Finally, it should be possible to effectively

immobilize the target markers on the surface of the nanoparticles. For the detection of cancer marker-protein, due to them being a new class of aptamer, biomarker-specific aptamers in particular have attracted tremendous attention as molecular probes. An aptamer is a single-stranded nucleic acid (RNA or DNA) which has unique characteristics when binding to its targets such as small molecules, proteins, and cells with high specificity and selectivity [18–20]. Moreover, there are other advantages for biomolecular detection using aptamers, namely: high stability, low toxicity, low molecular weight, easy and standardized synthesis, and rapid tissue penetration. Furthermore, because aptamers can easily be conjugated with other molecules, there are many aptamer derivatives, such as aptamer dyes, aptamer drugs and aptamer aptamers [21–23]. These features make aptamers ideal alternatives to antibodies for various applications, including clinical diagnosis, therapy, and prognosis [24–26].

Herein, we have thus developed immuno-nanoplasmonics composed of systemic aptamer-integrated nanoprobes to measure and assess the sensing efficiency for target biomarkers. Immuno-nanoplasmonics consist of uniform silver nanomarbles (SNMs) that are sequentially functionalized with caffeic acid and chemisorbed epithelial cell adhesion molecule (EpCAM)-specific aptamers (figure 1). EpCAMs, also known as ESAs, are glycosylated, transmembrane proteins that are overexpressed in stem-like cancer cells [27–29], so they are known to be ideal biomarkers for cancer diagnosis, therapy, and prognosis [30–32]. For this reason, the detection of EpCAMs is emerging as an important issue in biomedical fields. SNMs have a larger FOM value than other metal nanoparticles such as gold or copper [17, 33], so the LSPR signal of an SNM has a tendency to display high accuracy and precision as the refractive index (RI) of the surrounding environment changes. To confirm the sensing capability of immuno-nanoplasmonics regarding specificity, selectivity, and stability for the biomarker, the LSPR signal was measured and verified using whole cell lysates obtained from various cancer cell lines. The four cell lines have been selected according to their cellular molecular characteristics that represent a more biologically relevant basis for molecular medicine. These cancer cell lines can be typically used for physiologically relevant cancer *in vitro* models based on surface-receptors and protein expressions. HEK293T cells derived from normal tissue-derived epithelial-like cells have significant implications for experiments that are used as control cells to compare with tumor-derived cell lines (MCF7, MDA-MB-231, and HT1080 cells). Single-nanoparticle scattering analysis by the nanoscattering spectrum imaging analysis (NSSIA) system was used in this approach. Sensing with single nanoparticles has received significant attention due to its ability to greatly increase the sensitivity of analyte sensing, that is to say, the absolute detection limit (numbers of analyte molecules per nanoparticle) is dramatically reduced [34]. Moreover, since only a few nanoparticles need to be monitored at a time, the required sample volume is significantly lower than for ensemble methods. Using these properties, there have been several demonstrations of bioimaging and biosensing on the scattering of a single nanoparticle [34–38].

2. Materials and methods

2.1. Materials

Diethylene glycol, sodium hydrosulfide, aqueous hydrochloric acid (37%), poly(vinyl pyrrolidone) (55 000 Da), silver trifluoroacetate, 3-aminopropyltriethoxysilane, and caffeic acid were all purchased from Sigma-Aldrich. N-hydroxysulfosuccinimide and 3-(3-dimethylaminopropyl)-carbodiimide were obtained from Pierce. The 3′-amine-modified anti-EpCAM DNA aptamer (5′-AGC GTC GAA TAC CAC TAC AGA GGT TGC GTC TGT CCC ACG TTG TCA TGG GGG GTT GGC CTG CTA ATG GAGC TCG TGG TCA G-NH_2-3′) was obtained from Aptamer Science Inc. [20]. Dulbecco's phosphate-buffered saline (PBS, 1 M, pH 7.4) was purchased from Welgene. All other chemicals and reagents were of analytical grade. Ultrapure deionized water (DW) was used for all synthesis processes. All glassware used in the experiments was cleaned in freshly prepared aqua regia solution and rinsed thoroughly in distilled water before use.

2.2. Fabrication of immuno-nanoplasmonics based on silver nanomarbles

Silver nanomarbles (SNMs), for the manufacturing of the LSPR sensor substrate, were synthesized by using a polyol reduction method with some modifications [39]. In detail, 5 ml of diethylene glycol in a 30 ml vial was heated to 150 °C under gentle stirring. Sodium hydrosulfide (3 mM, 60 μl), hydrochloride (3 mM, 500 μl), and poly(vinyl pyrrolidone) (0.36 nM, 1.25 ml) were sequentially dropped into pre-heated diethylene glycol. After further mixing for 2 min, a precursor silver trifluoroacetate solution (282 mM, 0.4 ml) was added and the vial was blocked for 30 min. To cease the inhomogeneous growth of the SNMs, the reaction solution was quickly chilled. The synthesized SNMs were gathered and purified by repeated centrifugation (15 000 rpm, 30 min). The washed SNMs were dispersed in 5 ml of DW. The shape and size of the synthesized SNMs were analyzed using transmission electron microscopy (TEM, JSM1011, JEOL Ltd). In addition, their absorbance spectrum was determined by a UV–vis spectrophotometer (Lamda 25, Perkin Elmer).

The LSPR sensor substrate was fabricated using the protocol of a previously published report [38]. A glass slide (12 mm) was cleaned in piranha solution (3:1 H_2SO_4/30% H_2O_2), thoroughly rinsed with DW three times and dried. To prepare the immuno-nanoplasmonics, the neat slide was then immersed in 5 ml of DW containing 100 μl of 3-aminopropyltriethoxysilane solution for 4 h. After the reaction, the slide was rinsed with an excess of DW and ethanol and dried. Subsequently, the aminated slide was immersed in 100 μl of SNM solution (4.98 mg of Ag ml^{-1}). After 24 h, the SNM-coated slide was repeatedly rinsed with

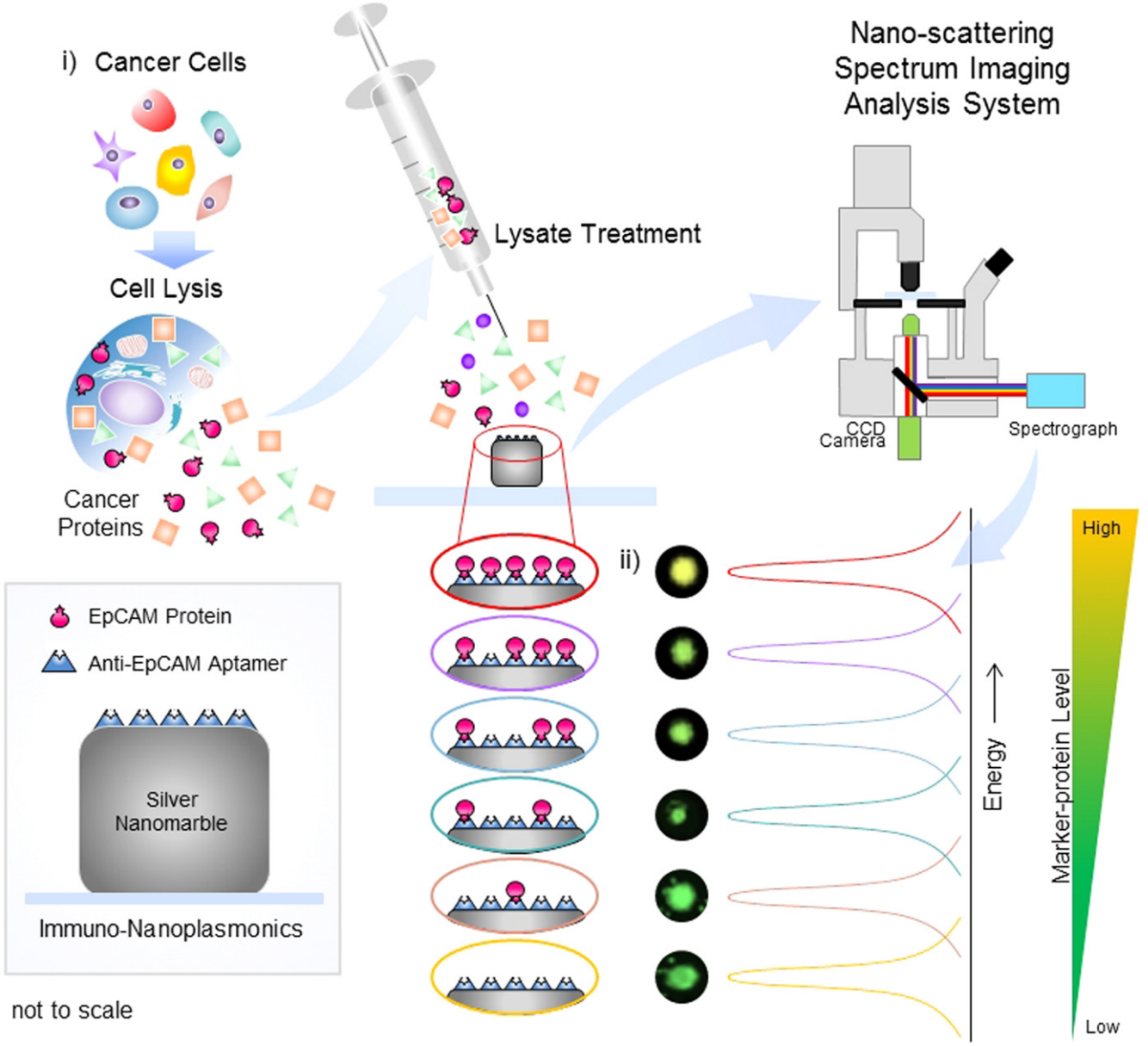

Figure 1. Schematics for precise analysis of cancer biomarker based on immuno-nanoplasmonics (anti-EpCAM aptamer-conjugated silver nanomarble) and the nanoscattering spectrum imaging analysis (NSSIA) system. (i) The extracted cancer proteins containing epithelial cell adhesion molecules (EpCAMs) from target cancer cells are treated with immuno-SNMs (iSNMs) for LSPR-based protein sensing. (ii) Energy grading of represented specific color from the LSPR signal by using NSSIA for the analysis of biomarker expressions.

DW and was then immersed into a solution that contained 100 μl of 2 μM caffeic acid. To fabricate the anti-EpCAM aptamer-conjugated SNM as an immuno-nanoplasmonic, EDC (2.3 μmol), sulfo-NHS (2.4 μmol), and anti-EpCAM DNA aptamer (1 μM, 100 μl) were reacted for 12 h and then washed with PBS (1 M, pH 7.4).

2.3. Nanoscattering spectrum imaging analysis (NSSIA) system

All scattering spectroscopic measurements and imaging for the optical nanoparticles were performed using a nanoscattering spectrum imaging analysis (NSSIA) system based on an inverted microscope (Axio Observer A1, Carl Zeiss) equipped with an imaging spectrograph (Acton SP2500, Princeton Instruments) and charge-coupled device (CCD) detector (PIXIS400B, Princeton Instruments). A color CCD camera (Thorlabs, DCU224C) was also attached to the front port of the microscope to facilitate the identification and alignment of the SNM. A dark field condenser (NA = 1.2–1.4) was used to illuminate the SNM and a variable aperture 40× objective (NA = 0.6–1.5) was used to collect the light scattered by them. The method for the measurement of the Rayleigh scattering spectra of a single SNM has been described in previous studies [34, 40]. Briefly, the spectrograph grating was placed in zero order and the spectrograph entrance slit was opened to its maximum setting in order to project a wide-field image onto the CCD detector.

Next, one SNM was placed in the center of the field and the entrance slit was closed to 20 μm. Then, the spectrograph grating was rotated to disperse first-order diffracted light onto the CCD detector. To ensure that only the scattered light from a single nanoparticle was analyzed, the region of interest was selected using CCD control software. An adjacent empty region of the CCD detector with the same dimensions was also collected in order to perform a background subtraction. Integration times varied depending on the lamp intensity and the scattering strength of the SNM, but a typical acquisition comprised of the accumulation of five exposures, each 5 s in duration. Finally, the raw scattering spectrum was normalized to correct for the lamp spectral profile, spectrograph throughput, and efficiency of the CCD detector. This was accomplished by dividing the raw spectrum by the lamp spectrum, which was obtained by increasing the numerical aperture of the objective above 1.4.

2.4. Cell culture and EpCAM expression level analysis

All target cancer cell lines used in this study were obtained from the American Type Culture Collection. The human breast cancer cell line, MDA-MB-231 cells, were maintained in RPMI1640 with 5% FBS, and the MCF7 cells were maintained in DMEM with 10% FBS. HT1080 cells, the human fibrosarcoma cell line, were cultured in MEM with 10% FBS, and the HEK293T cells, the human embryonic kidney cell line, were cultured in DMEM with 10% FBS. For the preparation of the whole cell lysates, the cells were rinsed with PBS to remove residual media. 1×10^6 cells were collected by centrifugation at 1100 rpm at room temperature for 3 min. The pellets were washed with PBS and again collected by centrifugation with the addition of 1 ml of 1× radioimmunoprecipitation assay (RIPA) buffer immediately after washing. The EpCAM expression level was analyzed using flow cytometry (fluorescence-activated cell sorting, FACS) and enzyme-linked immunosorbent assay (ELISA) according to the standard procedures. In detail, the cells in the experiments were dissociated using TrypLE Express (GIBCO), washed with PBS and incubated in blocking solution (1X PBS, 0.1% bovine serum albumin, 0.001% sodium azide). The cells were then incubated with 1 μl fluorescein isothiocyanate-conjugated anti-EpCAM antibodies (ESA214, GeneTex) for 30 min at 4 °C according to the manufacturer's protocols prior to the FACS analyses. Following incubation, the unattached antibodies were removed by washing with a blocking solution and the cell samples were fixed with 300 μl of 4% paraformaldehyde (Biosesang). Flow cytometry was performed using BD FACSCalibur (BD Bioscience) and the flow cytometric data was gated and displayed using WinMDI 3.9. For the quantitative measurement of human EpCAMs in cell culture supernatant, a commercial ELISA kit (ab155442, Abcam) was used as instructed. 96–well ELISA plates were coated with human EpCAMs (TROP1) with 50 ng standards and samples/well for 2.5 h at room temperature by gentle shaking. The wells were washed and biotinylated anti-human EpCAM (TROP1) antibodies were added and incubated for 1 h at room temperature with gentle shaking. After washing the unbound biotinylated antibodies, HRP-conjugated streptavidins were added to the wells and incubated for 45 min at room temperature with gentle shaking. The plate was rewashed and incubated with a TMB substrate solution for 30 min at room temperature in the dark with gentle shaking for the color to develop in proportion to the amount of EpCAM bound. Finally, the stop solution changed color from blue to yellow and was measured at 450 nm by a microplate spectrophotometer (Epoch, BioTek, USA).

3. Results and discussion

To prepare the LSPR sensing substrate for the sensitive detection of EpCAMs, the SNM was preferentially synthesized using the polyol reduction method with some modifications [39, 41, 42]. The size and morphology of the SNM was investigated using transmission electron microscopic imaging (figure 2(a)). The absorbance spectrum was recorded from an aqueous suspension of the SNMs (figure S1(a)), and the color of the suspension was yellow. The spectrum had a peak at 3.10 eV and the full width at half maximum (FWHM) was 0.23 eV. The FWHM value of the SNM is exceedingly low compared with nanoparticles composed of other materials, such as gold (6.2–20.7 eV) and copper (3.8–10.3 eV) [43, 44]. Because the small FWHM value correlates with the high value of the FOM of the LSPR sensor, the obtained 0.23 eV of the FWHM value represents the precise sensing potential for the NSSIA system. Subsequently, the SNM was immobilized on an amine-modified glass slide, and the attached SNM was observed via light scattering microscopic images. As can be seen in figure 2(b), the immobilized SNM on the aminated glass was observed as blue dots in the air due to its optical properties—especially in absorbance and scattering. In the absorbance spectrum of the SNM in figure S1(a) there is a peak at about 3.10 eV, so the SNM-immobilized glass substrate strongly absorbed light corresponding to 3.10 eV. Because the SNM absorbed light at 3.10 eV strongly, it scattered light that had almost the same energy. Subsequently, the LSPR sensitivity of the local RI for the bare SNM-attached glass substrate was investigated by the measurement of the spectra for single-nanoparticles using various dielectric media having a different RI, i.e. air: 1.00, water: 1.33, ethanol: 1.36, 1-propanol: 1.39, dimethylformaimde: 1.43 and chloroform: 1.49 (figure 2(c)). As the RI of the surrounding dielectric media was increased, the peak energy (E_{max}) of the scattering spectra was red-shifted. Moreover, the sensitivity of the sensing substrate which contained the attached SNMs also calculated the changes in the RI of the surrounding dielectric media; the sensitivity of the sensing substrate yielded 0.97 eV RI unit^{-1} (RIU) (figure 2(d)). We also imaged the single SNM using light scattering microscopic imaging, and the single SNM with a bluish-green color in the microscopic image has a λ_{max} at 2.48 eV (figure 2(e)). After the sequential functionalization of the SNM with caffeic acid and the aminated anti-EpCAM aptamer (as iSNM), the peak of the scattering signal was red-shifted towards 2.38 eV

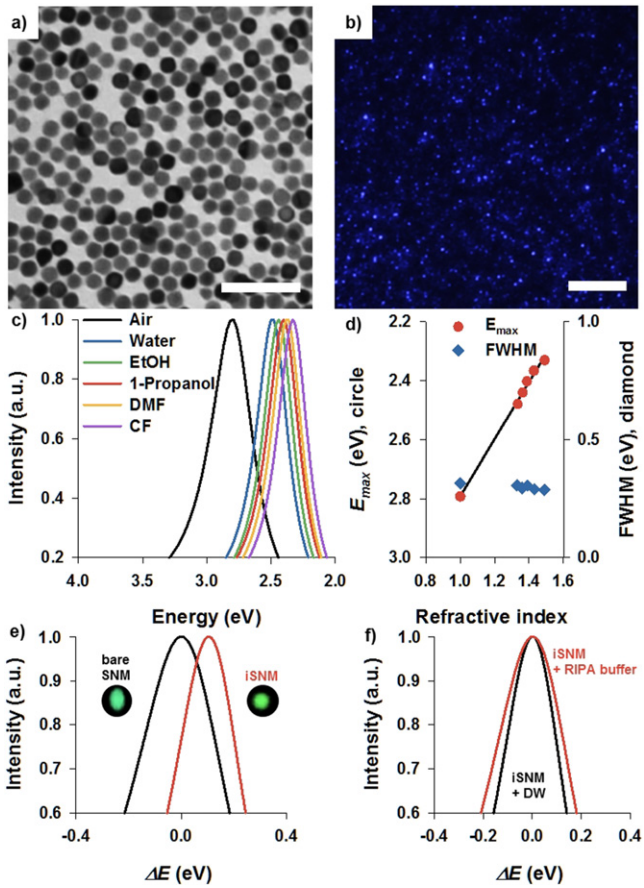

Figure 2. (a) Transmission electron microscopic image of SNMs; the scale bar is 100 nm. (b) Single-nanoparticle light scattering microscopic image of SNMs attached to a glass slide; the scale bar is 10 μm. (c) Scattering spectra of a single SNM in various media. (d) A plot describing the LSPR sensitivity of the single SNM and revealing the linear relationship between the media refractive index and the LSPR maximum energy, E_{max} (red circle) and FWHM plot for single SNM under each medium (dark blue diamond). (e) Single-nanoparticle light scattering spectra for single bare SNM (black) and anti-EpCAM aptamer-conjugated SNM (iSNM, red). The insets correspond to the single-nanoparticle light scattering microscopic images of bare SNMs (upper) and iSNMs (lower). (f) Single-nanoparticle light scattering spectra for iSNMs in DW (black) and in RIPA buffer (dark blue), respectively.

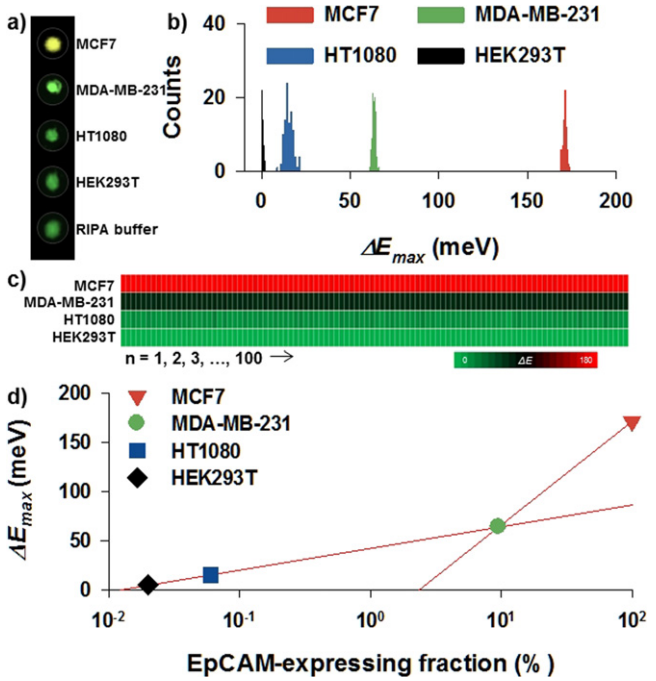

Figure 3. (a) Single-nanoparticle light scattering microscopic images of iSNMs treated with whole cancer cell lysates obtained from target cancer cells (MCF7, MDA-MB-231, HT1080, and HEK293T, respectively). (b) A histogram and (c) heat map for the shift of the LSPR maximum energy, ΔE_{max}, which is derived from the original peak position of the iSNMs in the RIPA buffer, for all of the cancer cell lines ($n = 100$). (d) Correlation graph between the LSPR energy peak shift (ΔE_{max}) and EpCAM-expression cell fractions (%) obtained by flow cytometry.

and the corresponding light scattering microscopic image showed a bright green color. As a control experiment, the scattering spectra were measured for iSNMs in deionized water and in the cell lysis RIPA buffer, respectively (figure 2(f); see also figures S1(b) and S1(c)). For both cases, the scattering signals scarcely shifted, and the changes in signals were negligible.

To investigate the sensing capability of iSNMs as immuno-nanoplasmonics for the detection of the EpCAM protein extracted from various live cancer cell lines (breast cancer cell lines; MCF7 and MDA-MB-231, fibrosarcoma cell line; HT1080 cells) and human embryonic kidney cell line (HEK293T cells), the light scattering microscopic images for the iSNMs treated with each whole cell lysate were obtained using light scattering images. As mentioned earlier, the four cell lines were selected according to their cellular molecular characteristics. The bright green dots of non-treated iSNMs in light scattering microscopic images turned yellow for the treatment of the lysate from MCF7 cells. For a detailed confirmation of the EpCAM detection capability of iSNMs, high-magnification single-nanoparticle light scattering microscopic images were investigated (figure 3(a)). Subsequently, the single-nanoparticle light scattering signals of the iSNMs using the NSSIA system for the single iSNM ($n = 100$) were analyzed after the treatment of each cell lysate (figures 3(b) and S2). The reference position for figure 3(b) was derived from the original position of the maximum peak of the iSNM treated with the RIPA buffer. The following shift values of the LSPR signal for each cell lysate were calculated from the original position of the iSNM treated with the RIPA buffer. The MCF7 cells exhibited the most significant LSPR signal shift (171.0 $\pm$ 1.1 meV), followed by the MDA-MB-231 (63.3 $\pm$ 0.9 meV), HT1080 (15.2 $\pm$ 2.4 meV), and HEK293T (0.5 $\pm$ 0.4 nm) cells. The heat map was depicted by using the obtained LSPR signals (figure 3(c)). These results indicate that iSNMs are capable of the detection of EpCAM protein without critical variations. Finally, flow cytometry analysis was also carried out for comparison with the measured LSPR signals (figures 3(d) and S3). The expression levels of the EpCAMs from each cancer cell line coincided with the results obtained by the LSPR sensor based on the iSNMs. The correlation graph shown in figure 3(d) can be divided into two subgroups, HEK293T to

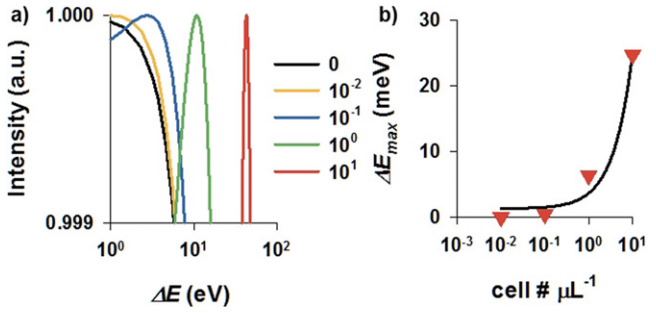

Figure 4. (a) The average single-nanoparticle light scattering spectra ($n = 100$) of a single iSNM after the treatment of the MCF7 cell lysate at the indicated cell concentration (cell # μl^{-1}). (b) The determination of the limit-of-detection (LOD) for EpCAMs with various cell concentrations (cell # μl^{-1}) and following the eventual LSPR energy peak shift (ΔE_{max}).

MDA-MB-231 being the first part, and from MDA-MB-231 to MCF7 being the second part for the linear fitting lines. Here, the ΔE_{max} obtained from the LSPR sensor of the single iSNM was clearly distinguished at each EpCAM expression level after the lysis of each cancer cell. However, flow cytometry analysis basically detects the marker-expressing cells using fluorescent targeting moiety binding with the cell surface marker. These results suggest that our iSNM sensor system can detect the expression level of a specific biomarker that exists in a whole cell lysate.

In addition, iSNMs have considerable selectivity and sensitivity for the EpCAM protein extracted from each cancer cell. Furthermore, the limit-of- detection (LOD) of the iSNM sensor system was studied for large LSPR signal cancer cell lines (MCF7 cells). LOD tests for MCF7 cells demonstrate that the combination of iSNMs and the NSSIA system can detect target biomarkers, EpCAMs, at a single-cell level. The ΔE_{max} value at a concentration of one cell per microliter (μl) was 6.4 meV. Even so, the centesimal cellular concentration (10^{-2} cell # μl^{-1}) was remarkably differentiable based on the measured LSPR spectrum of the iSNMs (figure 4(a)). For the determination of the detection limit for EpCAM molecules via iSNMs and the NSSIA system, the conventional quantitative analysis of EpCAM amounts was preferentially processed via enzyme-linked immunosorbent assay (ELISA). The EpCAM amount in one MCF7 cell was measured with 0.23 pg and a molar amount of EpCAM (34 932 Da) was calculated with 6.7 atto moles per one cell. As shown in figure 4(b), in particular, in the case of the 10^{-2} cell # μl^{-1} condition, detection corresponds to 67 fM of the EpCAM proteins, respectively. From the measured values from the ELISA and NSSIA system, the latter can detect the expression levels of specific proteins, such as EpCAMs, at the femtomolar level for single-cell levels.

4. Conclusions

In conclusion, we have developed a systemic LSPR sensor composed of SNMs modified with an EpCAM-specific aptamer, and the NSSIA system for sensitive biomarker detection. The SNMs synthesized using the polyol method have a large FOM value, so the changes in the LSPR signal by the variation of RI can be well measured and modified with biomarker-capturing aptamers using a simple bioconjugation chemistry as 'immuno-nanoplasmonics'. In particular, the NSSIA system for single-nanoparticle spectrum analysis has successfully been used as a method for maximizing LSPR sensitivity for target cancer biomolecular detection in a single cell, that is to say, at femto-molar levels for EpCAM proteins. Using this integrative LSPR sensor system, we have classified the various cancer cell lines against the expression level of EpCAM proteins. Collectively, we have verified the sensing capability for the specific and sensitive detection of biomarkers—the EpCAM protein that exists within stem-like cancer cells—using an iSNM-based LSPR sensor system on whole lysates obtained from cancer cells.

Acknowledgments

This work was supported by the National Research Foundation of Korea (NRF) funded by the Ministry of Science, ICT and Future Planning (2012R1A11006248 and 2014R1A1A2059806).

References

[1] Stern E, Vacic A, Rajan N K, Criscione J M, Park J, Ilic B R, Mooney D J, Reed M A and Fahmy T M 2010 *Nat. Nanotechnol.* **5** 138–42
[2] Tabakman S M *et al* 2011 *Nat. Commun.* **2** 466
[3] Rodríguez-Lorenzo L, de la Rica R, Álvarez-Puebla R A, Liz-Marzán L M and Stevens M M 2012 *Nat. Mater.* **11** 604–7
[4] Choi C *et al* 2012 *Nat. Med.* **18** 624–9
[5] Hindson C M, Chevillet J R, Briggs H A, Gallichotte E N, Ruf I K, Hindson B J, Vessella R L and Tewari M 2013 *Nat. Methods* **10** 1003–5
[6] Ito H, Inoue H, Hasegawa K, Hasegawa Y, Shimizu T, Kimura S, Onimaru M, Ikeda H and Kudo S-E 2014 *Nanomed-Nanotechnol.* **10** 599–608
[7] Anker J N, Hall W P, Lyandres O, Shah N C, Zhao J and Van Duyne R P 2008 *Nat. Mater.* **7** 442–53
[8] Kabashin A V, Evans P, Pastkovsky S, Hendren W, Wurtz G A, Atkinson R, Pollard R, Podolskiy V A and Zayats A V 2009 *Nat. Mater.* **8** 867–71
[9] Brolo A G 2012 *Nat. Photon.* **6** 709–13
[10] Xiong B, Zhou R, Hao J, Jia Y, He Y and Yeung E S 2013 *Nat. Commun.* **4** 1708
[11] Zhang L, Li Y, Li D-W, Jing C, Chen X, Lv M, Huang Q, Long Y-T and Willner I 2011 *Angew. Chem. Int. Ed.* **50** 6789–92
[12] Shi L, Jing C, Ma W, Li D-W, Halls J E, Marken F and Long Y-T 2013 *Angew. Chem. Int. Ed.* **52** 6011–4
[13] Hong Y, Huh Y-M, Yoon D S and Yang J 2012 *J. Nanomater.* **2012** 758930
[14] Zhao J, Zhang X, Yonzon C R, Haes A J and Van Duyne R P 2006 *Nanomedicine* **1** 219–28
[15] Sepúlveda B, Angelomé P C, Lechuga L M and Liz-Marzán L M 2009 *Nano Today* **4** 244–51
[16] Mayer K M and Hafner J H 2011 *Chem. Rev.* **111** 3828–57

[17] Sagle L B, Ruvuna L K, Ruemmele J A and Van Duyne R P 2011 *Nanomedicine* **6** 1447–62
[18] Shangguan D, Li Y, Tang Z, Cao Z C, Chen H W, Mallikaratchy P, Sefah K, Yang C J and Tan W 2006 *Proc. Natl Acad. Sci. USA* **103** 11838–43
[19] Mi J, Liu Y, Rabbani Z N, Yang Z, Urban J H, Sullenger B A and Clary B M 2010 *Nat. Chem. Biol.* **6** 22–4
[20] Song Y, Zhu Z, An Y, Zhang W, Zhang H, Liu D, Yu C, Duan W and Yang C J 2013 *Anal. Chem.* **85** 4141–9
[21] Vinkenborg J L, Karnowski N and Famulok M 2011 *Nat. Chem. Biol.* **7** 519–27
[22] Yang L, Zhang X, Ye M, Jiang J, Yang R, Fu T, Chen Y, Wang K, Liu C and Tan W 2011 *Adv. Drug Delivery Rev.* **63** 1361–70
[23] Bunka D H J and Stockley P G 2006 *Nat. Rev. Microbiol.* **4** 588–96
[24] Keefe A D, Pai S and Ellington A 2010 *Nat. Rev. Drug Discov.* **9** 537–50
[25] Iliuk A B, Hu L and Tao W A 2011 *Anal. Chem.* **83** 4440–52
[26] Famulok M and Mayer G 2011 *Acc. Chem. Res.* **44** 1349–58
[27] Visvader J E and Lindeman G J 2008 *Nat. Rev. Cancer* **8** 755–68
[28] Visvader J E and Lindeman G J 2009 *Nat. Rev. Cancer* **9** 143–143
[29] Shigdar S, Lin J, Yu Y, Pastuovic M, Wei M and Duan W 2011 *Cancer Sci.* **102** 991–8
[30] Nagrath S *et al* 2007 *Nature* **450** 1235–9
[31] Osta W A, Chen Y, Mikhitarian K, Mitas M, Salem M, Hannun Y A, Cole D J and Gillanders W E 2004 *Cancer Res.* **64** 5818–24
[32] Yamashita T *et al* 2008 *Cancer Res.* **68** 1451–61
[33] Ringe E, McMahon J M, Sohn K, Cobley C, Xia Y, Huang J, Schatz G C, Marks L D and Van Duyne R P 2010 *J. Phys. Chem.* C **114** 12511–6
[34] McFarland A D and Van Duyne R P 2003 *Nano Lett.* **3** 1057–62
[35] Nan X, Sims P A and Xie X S 2008 *Chem. Phys. Chem.* **9** 707–12
[36] Ueno H, Nishikawa S, Iino R, Tabata K V, Sakakihara S, Yanagida T and Noji H 2010 *Biophys. J.* **98** 2014–23
[37] Sagle L B, Ruvuna L K, Ruemmele J A and Van Duyne R P 2011 *Nanomedicine* **6** 1447–62
[38] Hong Y, Ku M, Lee E, Suh J-S, Huh Y-M, Yoon D S and Yang J 2014 *J. Biomed. Opt.* **19** 051202
[39] Wang Y, Zheng Y, Huang C Z and Xia Y 2013 *J. Am. Chem. Soc.* **135** 1941–51
[40] Hong Y, Hwang S, Yoon D S and Yang J 2015 *Sensors Actuators* B **218** 31–6
[41] Sun Y and Xia Y 2002 *Science* **298** 2176–9
[42] Im S H, Lee Y T, Wiley B and Xia Y 2005 *Angew. Chem. Int. Ed.* **44** 2154–7
[43] Zhu J 2005 *Phys. Lett.* A **339** 466–71
[44] Bansal A and Verma S S 2014 *AIP Adv.* **4** 0571